



21 **Abstract**

22 Emissions of ozone (O₃) precursors in the United States have decreased
23 in recent decades, and near-surface O₃ concentrations showed a significant
24 decrease in summer but an increase in winter. In this study, an O₃ source
25 tagging technique is utilized in a chemistry-climate model to investigate the
26 source contributions to O₃ concentrations in the U.S. from various emitting
27 sectors and regions of nitrogen oxides (NO_x) and reactive carbon species
28 during 1995–2019. We show that domestic emission reductions from energy
29 and surface transportation are primarily responsible for the decrease in
30 summertime O₃ during 1995–2019. However, in winter the emission control also
31 weakens the NO_x titration process, resulting in considerable increases in O₃
32 levels from natural sources. Additionally, increases in aviation and shipping
33 activities and transpacific transport of O₃ from Asia largely contribute to the
34 winter O₃ increase. Changes in large-scale circulation also explain 15% of the
35 O₃ increasing trend.



36 **1. Introduction**

37 Ozone (O_3) near the surface has a significant impact on air quality and
38 public health (Haagen-Smit, 1952; Fleming et al., 2018). Since the increase in
39 anthropogenic emissions of O_3 precursors from preindustrial times, O_3 has now
40 become the third most important anthropogenic greenhouse gas in the
41 troposphere (Myhre et al., 2013). Major sources of O_3 in the troposphere
42 include the transport from the stratosphere and formation through
43 photochemical reactions within the troposphere involving two chemically
44 distinct groups of precursors: nitrogen oxides (NO_x) and reactive carbon
45 species, including carbon monoxide (CO), methane (CH_4), and non-methane
46 volatile organic compounds (NMVOCs) (Atkinson, 2000). O_3 precursors come
47 from a variety of sectors, and its relatively long lifetime of about 22 days
48 (Stevenson et al. 2006) favors the long-range transport of O_3 . Due to the
49 nonlinearity of the O_3 production and its associated dependence on precursor
50 emissions (Seinfeld and Pandis, 1997), attributing O_3 pollution to its sources is
51 complicated.

52 Since the 1980s, O_3 precursor emissions have significantly reduced in the
53 United States (Duncan et al., 2016; Xing et al., 2013; Zhang et al., 2016; Zhang
54 et al., 2021). However, due to the nonlinear production chemistry of O_3 ,
55 complex seasonal meteorological influence, and long-range transport from
56 foreign source regions, domestic emissions reductions do not imply a decrease
57 in seasonal and annual O_3 concentrations. According to remote surface
58 measurements (Cooper et al., 2020) and aircraft observations (Gaudel et al.,
59 2020), the Sixth Assessment Report of the Intergovernmental Panel on Climate
60 Change (Szopa et al., 2021) showed a decreasing trend in annual mean O_3
61 concentrations in the western U.S. but an increasing trend in the eastern U.S.
62 since the mid-1990s. On the seasonal timescale, surface observations and
63 modeling results showed that O_3 concentrations over the U.S. had decreased



64 in summer due to the reductions in domestic anthropogenic emissions and
65 increased in winter related to the weakened NO_x titration since the late 1980s
66 (Cooper et al., 2012; Lin et al., 2017). It also shows that the increased
67 background O₃, especially due to an increased transport from Asia, can partly
68 offset the benefit of domestic emissions control over the western U.S. in
69 summer.

70 Source apportionment is a useful method for quantifying contributions to
71 air pollutants from specific source regions and/or sectors, which is beneficial to
72 emission control strategies (Yang et al., 2018). The traditional method of
73 obtaining an O₃ source-receptor relationship is to zero out or perturb emissions
74 from a given source region or sector in sensitivity simulations along with a
75 baseline simulation (e.g., Fiore et al., 2009; Hoor et al., 2009). However,
76 emission perturbation method requires many additional model simulations
77 when being used to estimate the contributions of multiple sources (Koo et al.,
78 2009; Wang et al., 2014) and the perturbation method may invalidate the
79 assumption of a linear relationship between the magnitude of the emission
80 perturbation and the magnitude of the O₃ change considering the nonlinearity
81 in O₃ chemistry, especially if large perturbations (e.g. zeroing out regional or
82 sector-wide emissions) are used. The tagging approach produces information
83 about the contribution of precursor emissions to the total amount of O₃, while
84 perturbation approach gives information about the response of O₃ to changes
85 in precursor emissions (Butler et al., 2020). Both of these two methods can be
86 used for specific purpose to provide a comprehensive understanding source-
87 receptor relationships between precursor emissions and O₃ concentrations.

88 The source tagging method has been widely adopted in regional air quality
89 models to examine the O₃ attribution in the U.S., China, and/or Europe (Collet
90 et al., 2022; Gao et al., 2016; Lupaşcu and Butler, 2019). In regional models,
91 O₃ apportionment is based on the ratio of chemical indicators to determine the



92 regime of O₃ generation (e.g., VOC-limited or NO_x-limited regimes) and then
93 attribute the generation of O₃ to the tag carried by a certain precursor (VOCs or
94 NO_x), which however cannot simultaneously attribute O₃ production to NO_x and
95 VOCs, respectively. In addition, due to the limitation in domain size of regional
96 air quality models, they are difficult to account for contributions of
97 intercontinental transport from sources outside the model domain. Recently, O₃
98 tagging techniques have been implemented in the global models (e.g., Bates
99 and Jacob, 2020; Han et al., 2018; Sudo and Akimoto, et al., 2007; Zhang et
100 al., 2008). However, in many global models, O₃ is tagged by the production
101 regions rather than the precursor emission regions, so that O₃ can only be
102 attributed to the area where O₃ is generated, rather than the source of precursor
103 emissions.

104 Here, based on a state-of-the-art tagging system implementation in a
105 global chemistry–climate model, the trends of near-surface O₃ concentrations
106 in the U.S. during 1995–2019 and the source attributions of the O₃ variations to
107 various emission sectors and regions of NO_x and reactive carbon species are
108 investigated in this study. Mechanisms of explaining the O₃ trends that involve
109 changes in anthropogenic emissions and large-scale circulations are also
110 explored.

111 **2. Methods**

112 **2.1 Model Description**

113 Tropospheric O₃ concentrations are simulated using the Community
114 Atmosphere Model version 4 with Chemistry (CAM4-chem) (Lamarque et al.,
115 2012; Tilmes et al., 2015), which is the atmospheric chemistry component of
116 the Community Earth System Model (CESM), at a horizontal resolution of 1.9°
117 latitude by 2.5° longitude with 26 vertical levels extending to 40 km above the
118 surface. The model configuration uses a comprehensive tropospheric
119 chemistry mechanism based on the Model for Ozone and Related chemical



120 Tracers version 4 (MOZART-4) (Emmons et al., 2010). Stratosphere-
121 troposphere exchange of O₃ is treated by setting O₃ to stratospheric values at
122 the tropopause, which experiences the same loss rates as O₃ in the
123 troposphere (Tilmes et al., 2016). Sea surface temperatures and sea ice
124 concentrations in our simulations are prescribed at present-day climatological
125 conditions. Model winds are nudged towards the MERRA-2 (Modern Era
126 Retrospective-Analysis for Research and Applications Version 2) reanalysis
127 (Gelaro et al., 2017) at a 6-hourly relaxation timescale in this study to better
128 constrain large-scale circulations by observations. The CAM4-chem
129 performance in simulating tropospheric O₃ and precursors has been fully
130 evaluated in Tilmes et al. (2015).

131 **2.2 Ozone Source Tagging Technique**

132 The novel O₃ source tagging technique implemented in the model was
133 developed by Butler et al. (2018), which can provide a separate source
134 apportionment of tropospheric O₃ to the two distinct groups of precursor
135 emissions, i.e., NO_x and reactive carbon (CO, CH₄ and NMVOCs). The portion
136 of tropospheric O₃ that is attributable to the stratosphere-troposphere exchange
137 can also be quantified using this unique tagging technique. The source
138 attribution of O₃ requires two separate model runs with the tagging applied to
139 NO_x and reactive carbon species, respectively. Details of the O₃ tagging
140 technique are described in Butler et al. (2018).

141 In this study, near-surface O₃ is attributed to emission sectors and regions.
142 Emissions from individual sectors, including agriculture (AGR), energy (ENE),
143 industry (IND), residential, commercial and other (RCO), surface transportation
144 (TRA), waste management (WST), international shipping (SHP) and biomass
145 burning (BMB) emissions, as well as chemical production in the stratosphere
146 (STR) and extra chemical production (XTR, a small amount of O₃ produced due
147 to the self-reaction of OH radicals and the reactions of HO₂ with certain organic



148 peroxy radicals) are tagged for both NO_x and reactive carbon species. Aircraft
149 (AIR), soil (SOIL) and lightning (LGT) sources are separately tagged for NO_x
150 emissions, while solvents (SLV) and biogenic (BIO) sources are separately
151 tagged for NMVOCs emissions.

152 For the regional source attribution, we separately tag anthropogenic
153 sources from Africa (AFR), Central America (CAM), Europe (EUR), Middle East
154 (MDE), North America (NAM), East Asia (EAS), South Asia (SAS), Southeast
155 Asia (SEA) and rest of the world (ROW) (see Fig. 1 for the region map) and
156 natural sources (BMB, SOIL, LGT, BIO, STR and XTR). Additional tags for
157 methane (CH₄) and carbon monoxide (CO) are applied in both of the reactive
158 carbon tagging simulations that are used to attribute O₃ to emission sectors and
159 regions. We did not tag CH₄ and CO by individual sources, because CH₄ is
160 often considered separately from NMVOCs. It has a relative long lifetime in the
161 troposphere and it is well mixed in the troposphere due to its exceptionally low
162 reactivity, which can contribute to O₃ formation at any location in the
163 troposphere where photochemical conditions are favorable (Fiore et al., 2008).
164 CO also has a longer lifetime and lower reactivity than most NMVOCs. On the
165 other hand, the number of tags is limited by the complexity of chemical
166 mechanism.

167 **2.3 Emissions and Observation**

168 The global anthropogenic emissions, including NO_x, CO and NMVOCs,
169 over 1990–2019 are from the Community Emissions Data System (CEDs)
170 version 20210205 (Hoesly et al., 2018). Biomass burning emissions are
171 obtained from the CMIP6 (Coupled Model Intercomparison Project Phase 6)
172 over 1990–2014 (van Marle et al., 2017) and the emissions for the following five
173 years (2015–2019) are interpolated from the SSP2-4.5 forcing scenario (O'Neill
174 et al., 2016). NO_x emitted from soils and biogenic NMVOCs from vegetation are
175 prescribed as in Tilmes et al. (2015) and are kept at the present-day



176 climatological levels during simulations. Lightning emissions of NO_x are
177 estimated based on the Price parameterization (Price et al., 1997). CH_4
178 concentration is fixed at a global average of 1750 parts per billion (ppb) during
179 simulations.

180 Surface O_3 measurements in the U.S. are obtained from the U.S.
181 Environmental Protection Agency (EPA). Linear trends of surface O_3 are
182 calculated separately for boreal summer (June-July-August, JJA) and winter
183 (December-January-February, DJF). Seasonal mean for any site that has less
184 than 50% data availability in any month of a season is not calculated. O_3 trends
185 at sites is shown only when the data availability is greater than 85% during the
186 analyzed period.

187 **2.3 Experimental Design**

188 In this study, four groups of experiments are conducted, each group
189 includes both NO_x tagging simulation and reactive carbon tagging simulation.
190 Two BASE experiment groups include simulations with emission sectors and
191 regions, respectively, tagged for the two chemical distinct precursors. The
192 BASE experiments are performed with time-varying anthropogenic emissions
193 and winds nudged to MERRA-2 reanalysis. The other two groups of sensitivity
194 experiments (MET) are the same as BASE experiments, except that the
195 anthropogenic emissions are held at year 2019 level during simulations. All
196 experiments are performed over 1990–2019, with the first 5 years treated as
197 model spin-up and the last 25 years used for analysis. The BASE experiments
198 are analyzed to quantify the source attributions of O_3 in the U.S., unless stated
199 otherwise.

200 **3 Results**

201 **3.1 Ground-level ozone trends in the U.S.**

202 Emissions of O_3 precursors have substantially reduced since 1995 in both
203 the western U.S. (WUS, 100–125°W, 30–45°N) and eastern U.S. (EUS, 70–



204 100°W, 30–45°N), primarily owing to the reductions in anthropogenic
205 emissions (Figs. S1–S3). However, the simulated annual near-surface O₃
206 concentrations present opposite trends between WUS and EUS, with increases
207 in EUS but weak decreases in WUS, which also exist in observations (Fig. 2a).

208 Looking at different seasons, we found the simulated contrasting trends in
209 annual mean O₃ concentrations between the WUS and EUS are dominated by
210 the strong decreases in O₃ concentrations in summer across the U.S. and
211 increased O₃ levels in winter over the central-eastern U.S. during 1995–2019.
212 The opposite trends between summer and winter have also been noted in many
213 previous studies (e.g., Copper et al., 2012; Lin et al., 2017, Jaffe et al., 2018).
214 CAM4-Chem can well reproduce the spatial distribution of the O₃ trends, with
215 spatial correlation coefficients of 0.70 in summer and 0.92 in winter between
216 observed and simulated trends in the continental U.S. during 1995–2019. The
217 model reproduces the observed O₃ trend of -3.0 ± 0.41 ppb/decade (linear trend
218 \pm standard error) over EUS in summer (-3.0 ± 0.29 ppb/decade in model) and
219 2.2 ± 0.23 ppb/decade over WUS in winter (3.2 ± 0.28 ppb/decade in model). The
220 decreasing trend over WUS in summer (-2.3 ± 0.20 ppb/decade in model v.s. $-$
221 0.5 ± 0.42 ppb/decade in observation) and increasing trend over EUS in winter
222 (6.1 ± 0.40 ppb/decade in model v.s. 2.1 ± 0.29 ppb/decade in observation),
223 however, are largely overestimated in the model. For spring and autumn, they
224 are the transition between summer and winter, having the similar spatial pattern
225 of O₃ trends as annual average, and will not be concerned in this study.

226 **3.2 Source attribution of ozone trends to emission sectors**

227 During 1995–2019, summer and winter NO_x emissions from energy and
228 surface transport sectors have significantly decreased in both WUS and EUS,
229 followed by industry and residential sectors, while those from aircraft have
230 increased slightly (Fig. 3). Emissions of NMVOCs from surface transportation,
231 solvents, industry, residential and waste sectors have decreased across the



232 U.S., while those from energy and agriculture have increased. CO emissions
233 have also significantly decreased over this time period.

234 The O₃ trends in the U.S. attributed to different emission source sectors
235 are shown in Fig. 5. The time series of the source contributions from NO_x and
236 reactive carbon emissions are shown in Figs. 4, respectively. In summer, the
237 O₃ attributed to energy and surface transportation NO_x emissions decreased at
238 the rate of 2.0±0.17 and 1.6±0.17 ppb/decade in WUS and 3.2±0.15 and
239 1.7±0.21 ppb/decade in EUS, respectively (Figs. 5a and 5c). On the contrary,
240 the O₃ contributed by aircraft NO_x emissions increased by 0.4±0.03 ppb/decade
241 in both WUS and EUS. Along with the reductions in anthropogenic emissions,
242 natural emissions are becoming increasingly important as sources for O₃
243 formation near the surface. Although NO_x emissions from soil are held at the
244 present-day climatological levels, they account for 0.7±0.08 and 1.7±0.10
245 ppb/decade increase in WUS and EUS, respectively, during 1995–2019, related
246 to the changing O₃ production efficiency under the more NO_x-sensitive
247 condition. In recent decades, emissions from international shipping have
248 increased rapidly (Eyring, 2005; Müller-Casseres et al., 2021), but the increase
249 has little impact on summer O₃ in the U.S. due to a strong chemical sink
250 associated with photolysis of O₃ with subsequent production of hydroxyl radical
251 (OH) from water vapor in summer (Johnson et al., 1999).

252 In summer, biogenic sources dominate the emissions of NMVOCs in the
253 U.S. (Fig. S3). As the O₃ decreases, mainly due to the reductions in domestic
254 NO_x emissions, the contributions from biogenic emissions of NMVOCs have a
255 decreasing trend in the U.S. during 1995–2019 (Figs. 5b and 5d), even though
256 biogenic emissions were fixed during simulations. This also applies to CH₄, of
257 which the concentration was kept constant. This does not actually mean that
258 CH₄ and biogenic NMVOCs themselves contributed to the overall O₃ trend;
259 rather, their O₃ production efficiency changed mainly due to changes in NO_x



260 emissions. In conjunction with NO_x emission reductions, decreases in NMVOCs
261 emissions from surface transportation and industry sectors contribute negative
262 O₃ trends of -0.3 ± 0.0 and -0.1 ± 0.0 ppb/decade, respectively, in both WUS and
263 EUS, which are offset by the increases in NMVOCs emissions from energy and
264 agriculture sectors. Although the O₃ production efficiency of CO is relatively low,
265 the contributions of CO to O₃ concentrations largely decreased with trends of $-$
266 0.6 ± 0.1 and -0.5 ± 0.1 ppb/decade in WUS and EUS, respectively, due to the
267 massive reduction in anthropogenic emissions of CO (Fig. S1).

268 In winter, through the weakened NO_x titration process (Gao et al., 2013;
269 Simon et al., 2015), the NO_x emission control causes an increase in O₃ levels
270 during 1995–2019, especially the contribution from surface transportation
271 (0.4 ± 0.0 ppb/decade in WUS and 0.8 ± 0.1 ppb/decade in EUS) (Figs. 5e and
272 5g). In the context of reduced NMVOCs emissions, only aircraft NO_x emissions
273 slightly increased, but O₃ attributed to aircraft NO_x emissions shows positive
274 trends as large as 0.4 ± 0.0 and 0.6 ± 0.0 ppb/decade in WUS and EUS,
275 respectively, because aircraft emissions are injected directly into the upper
276 troposphere and lower stratosphere in a low ambient NO_x condition and have
277 a much higher O₃ enhancement efficiency than surface emissions (Hodnebrog
278 et al., 2011). The increase in international shipping adds more NO_x to the
279 polluted boundary-layer environment and enhance the chemical production of
280 O₃ (Koffi et al., 2010), together with the weakened O₃ chemical sink from water
281 vapor in winter, leading to large increasing trends of O₃ by 0.8 ± 0.1 and 1.0 ± 0.1
282 ppb/decade, respectively, in the WUS and EUS during 1995–2019. Although
283 natural emissions do not change during the simulations, the net O₃ chemical
284 production is more sensitive to NO_x under the emission control condition,
285 resulting in the increasing O₃ trends contributed by the soil and lightning NO_x
286 emissions. Due to the weakened NO_x titration in winter, the contribution of
287 stratospheric intrusion increases at a rate of 0.6 ± 0.1 and 1.0 ± 0.1 ppb/decade



288 over WUS and EUS, respectively, when stratospheric contribution to the near-
289 surface O₃ reaches its maximum (Butler et al., 2018). Along with the weakened
290 NO_x titration, contributions from reactive carbon emissions to the near-surface
291 O₃ in the U.S. also increase for most species and sectors (Figs. 5f and 5h).

292 **3.3 Source attribution of ozone trends to emission regions**

293 The O₃ trends in the U.S. attributed to different emission source regions
294 are presented in Fig. 7. Time series of the source contributions are shown in
295 Figs. 6. In summer, domestic NO_x emissions within North America account for
296 53% of the near-surface O₃ concentration averaged over the U.S. (WUS+EUS)
297 in 1995–2019. The domestic emission reduction is the dominant factor causing
298 the decline in surface O₃ concentrations, with contributions of -3.7 ± 0.2 and $-$
299 4.7 ± 0.3 ppb/decade to the trends over WUS and EUS, respectively, during
300 1995–2019 (Figs. 7a and 7c). Reductions in the NMVOCs emissions from North
301 American anthropogenic sources also decrease O₃ concentrations (Figs. 7b
302 and 7d), accompanying with the domestic NO_x emission control. The increase
303 in NO_x emissions from Asia contributes 0.6 ± 0.1 ppb/decade to the total O₃
304 increasing trend in WUS, partly offsetting the negative impact of domestic
305 emission reductions, but has a weak impact in EUS, which is consistent with
306 previous studies (Lin et al., 2017).

307 In winter, domestic NO_x emissions only account for 19% of the surface O₃
308 concentration in the U.S. over 1995–2019, while NO_x sources from lightning,
309 rest of the world (mainly from the international shipping), and Asia contribute
310 17%, 14%, and 11%, respectively, and O₃ from stratospheric intrusion
311 contributes 21% of the near-surface O₃ in the U.S. (Fig. 6). During 1995–2019,
312 the significant increase in wintertime surface O₃ concentrations are not directly
313 linked to the reductions in domestic anthropogenic emissions (Figs. 7e and 7g).
314 However, the domestic emission control weakens the NO_x titration, resulting in
315 considerable increases in O₃ originating from the natural sources, including O₃



316 from stratospheric intrusion, lightning and soil emissions. The natural sources
317 combined contribute to positive O₃ trends of 1.1±0.2 and 2.3±0.3 ppb/decade
318 in WUS and EUS, respectively. If the O₃ increase is attributed to NMVOCs
319 emissions, the combined natural source contribution is even larger (1.4±0.2 and
320 2.5±0.2 ppb/decade) (Figs. 7f and 7h). O₃ produced by CH₄ increases at rates
321 of 1.3±0.1 and 2.1±0.1 ppb/decade in WUS and EUS, respectively, due to the
322 weakened NO_x titration. Increases in aviation and shipping emissions explain
323 the 1.2±0.1 and 1.5±0.1 ppb/decade of O₃ trends in WUS and EUS, respectively
324 (Figs. 5e and 5g). Long-range transport of O₃ produced from Asian NO_x
325 emissions enhances the wintertime O₃ increasing trends by 0.9±0.1 and
326 1.2±0.1 ppb/decade in WUS and EUS, respectively, which are equally
327 contributed by sources from East Asia, South Asia, and Southeast Asia (Figs.
328 7e and 7g).

329 **3.4. Impact of variations in large-scale circulations on ozone trends**

330 Many studies have reported that O₃ spatial distribution is strongly
331 modulated by changes in large-scale circulations (e.g., Shen and Mickley, 2017;
332 Yang et al., 2014, 2022). Based on our MET experiments with anthropogenic
333 emissions kept unchanged, the changes in large-scale circulations show a
334 weak influence on the U.S. O₃ trends in summer (Fig. 8a) but cause a significant
335 O₃ rise in the central U.S. in winter (Fig. 8b). Averaged over the U.S., the near-
336 surface O₃ concentration in winter increases at the rate of 0.7±0.3 ppb/decade
337 during 1995–2019 in MET experiments, accounting for 15% of the trend of
338 4.7±0.3 ppb/decade in BASE experiments. It suggests that the variation in
339 large-scale circulations is responsible for 15% of the increase in wintertime O₃
340 concentrations in the U.S. over 1995–2019.

341 The changes in atmospheric circulation pattern support the above finding.
342 Compared to 1995–1999, anomalous northerly winds locate over high latitudes
343 of North America in 2015–2019 (Fig. 8c), strengthening the prevailing northerly



344 winds in winter. The strengthened winds transport O₃ from high latitude regions
345 to the central U.S., causing an O₃ accumulation. In addition, an anomalous
346 subsidence also occurs over the central U.S. in 2015–2019, compared to 1995–
347 1999 (Fig. 8d), leading to an anomalous downward transport of O₃ from high
348 altitudes and even stratosphere to the surface. The horizontal and vertical
349 transport of O₃ together contribute to the near-surface O₃ increases in winter
350 during 1995–2019 associated with the changes in large-scale circulations.

351 **4. Conclusions and discussions**

352 Using a global chemistry–climate model equipped with an O₃ source
353 tagging technique, we examine the long-term trends and source apportionment
354 of O₃ in the continental U.S. over 1995–2019 to various emission source
355 sectors and regions in this study. This model can well capture the O₃ increasing
356 trend in summer and decreasing trend in winter over the U.S. during this time
357 period.

358 In summer, the decline in surface O₃ is dominated by the rapid reductions
359 in NO_x emissions from energy and surface transportation sectors, contributing
360 to O₃ decreases at a rate of –2.0 and –1.6 ppb/decade in WUS and –3.2 and –
361 1.7 ppb/decade in EUS, respectively. As the anthropogenic NO_x decreases, the
362 more NO_x-sensitive condition leads to a positive O₃ trend of 0.7 and 1.7
363 ppb/decade in WUS and EUS, respectively, contributed by the NO_x emissions
364 from soil. Due to the reductions in NO_x emissions, the contributions to O₃ from
365 reactive carbon species also decrease in summer during 1995–2019. Source
366 region tagging suggests that the domestic emission reductions are primarily
367 responsible for the decreasing trend in summertime near-surface O₃
368 concentrations in the U.S. during 1995–2019.

369 The mechanisms of wintertime O₃ increases over the U.S. are more
370 complex. First, the domestic emission control weakens the NO_x titration,
371 resulting in considerable increases in O₃ originating from natural sources,



372 including O₃ from stratospheric intrusion, lightning, soil and biogenic emissions.
373 The natural sources combined contribute a positive O₃ trend of more than 1 and
374 2 ppb/decade in WUS and EUS, respectively. Second, increases in aviation and
375 shipping emissions explain the 1.2 and 1.5 ppb/decade of O₃ trends in WUS
376 and EUS, respectively. Third, long-range transport of O₃ produced from Asian
377 NO_x emissions enhances the wintertime O₃ increasing trends by 0.9 and 1.2
378 ppb/decade in WUS and EUS, respectively. Fourth, the anomalous horizontal
379 and vertical transport of O₃ associated with the changes in large-scale
380 circulation contributes to the near-surface O₃ increases over the U.S. by 15%
381 in winter during 1995–2019.

382 Compared to observations, the decreasing trend of O₃ concentrations over
383 WUS in summer and increasing trend over EUS in winter are overestimated in
384 the CAM4-chem model. Note that, most O₃ monitors are located in urban areas
385 and these areas generate strong O₃ during the day and have strong oxidation
386 titration at night. The daily and grid averaged O₃ concentrations output by the
387 model could be inconsistent with the urban observations. Besides, Lin et al.
388 (2017) found that the contribution from increasing Asian emissions offsets that
389 from the U.S. emission reductions, resulting in a weak O₃ trend in WUS. In this
390 study, the Asian NO_x emissions only contribute to 0.6 ppb/decade of the total
391 positive trend in WUS in summer, much lower than the 3.7 ppb/decade increase
392 attributable to the domestic emission reductions, suggesting that the Asian
393 contribution to the O₃ trends in WUS is underestimated in this study. We also
394 found that the model did not capture the significant increase in summertime O₃
395 levels in China in recent years, which explains the low contribution from Asian
396 sources. The bias of O₃ simulation in China may also lead to a bias in the
397 wintertime O₃ trend over EUS. Additionally, international shipping can have a
398 disproportionately high influence on tropospheric O₃ due to the dispersed
399 nature of NO_x emissions (Butler et al., (2020); Kasibhatla et al., 2000; von



400 Glasow et al., 2003), together with the weakened NO_x titration, resulting in the
401 overestimation of O₃ trends. The fixed CH₄ concentration during simulations
402 also biased the modeled O₃ trends in this study.



403 **Author contributions.** YY designed the research; PL and SL performed
404 simulations; PL analyzed the data. All authors including HW, KL, PW, BL, and
405 HL discussed the results and wrote the paper.

406

407 **Code and data availability.** The CESM is maintained by NCAR and is provided
408 freely to the community. The ozone tagging code has been described by Butler
409 et al. (2018). The MERRA-2 reanalysis data are from NASA GESDISC data
410 (<https://goldsmr5.gesdisc.eosdis.nasa.gov/data/MERRA2/M2I6NVANA.5.12.4/>,
411 last access: 1 August 2022). The surface O₃ measurements in U.S. are
412 obtained from the U.S. Environmental Protection Agency
413 (https://aqs.epa.gov/aqsweb/airdata/download_files.html#Daily, last access: 1
414 August 2022). The modeling results are made available at
415 <https://doi.org/10.5281/zenodo.6891316> (last access: 1 August 2022).

416

417 **Acknowledgments**

418 HW acknowledges the support by the U.S. Department of Energy (DOE), Office
419 of Science, Office of Biological and Environmental Research (BER), as part of
420 the Earth and Environmental System Modeling program. The Pacific Northwest
421 National Laboratory (PNNL) is operated for DOE by the Battelle Memorial
422 Institute under contract DE-AC05-76RLO1830.

423

424 **Financial support.** This study was supported by the National Key Research
425 and Development Program of China (grant 2020YFA0607803 and
426 2019YFA0606800), the National Natural Science Foundation of China (grant
427 41975159), and Jiangsu Science Fund for Distinguished Young Scholars (grant
428 BK20211541).

429

430 **Competing interests.** The authors declare that they have no conflict of interest.

431



432 **References**

433

434 Atkinson, R.: Atmospheric chemistry of VOCs and NO_x, *Atmos. Environ.*, **34**,
435 2063-2101, [https://doi.org/10.1016/S1352-2310\(99\)00460-4](https://doi.org/10.1016/S1352-2310(99)00460-4), 2000.

436

437 Bates, K. H. and Jacob, D. J.: An Expanded Definition of the Odd Oxygen
438 Family for Tropospheric Ozone Budgets: Implications for Ozone Lifetime and
439 Stratospheric Influence, *Geophys. Res. Lett.*, **47**, e2019GL084486,
440 <https://doi.org/10.1029/2019gl084486>, 2020.

441

442 Butler, T., Lupascu, A., and Nalam, A.: Attribution of ground-level ozone to
443 anthropogenic and natural sources of nitrogen oxides and reactive carbon in a
444 global chemical transport model, *Atmos. Chem. Phys.*, **20**, 10707-10731,
445 <https://doi.org/10.5194/acp-20-10707-2020>, 2020.

446

447 Butler, T., Lupascu, A., Coates, J., and Zhu, a. S.: TOAST 1.0: Tropospheric
448 Ozone Attribution of Sources with Tagging for CESM 1.2.2, *Geosci. Model Dev*,
449 <https://doi.org/10.5194/gmd-11-2825-2018>, 2018.

450

451 Collet, S., Kidokoro, T., Karamchandani, P., Jung, J., and Shah, T.: Future year
452 ozone source attribution modeling study using CMAQ-ISAM, *J&AWMA*, **68**,
453 1239-1247 <https://doi.org/10.1080/10962247.2018.1496954>, 2018.

454

455 Cooper, O. R., Gao, R.-S., Tarasick, D., Leblanc, T., and Sweeney, C.: Long-
456 term ozone trends at rural ozone monitoring sites across the United States,
457 1990-2010, *J. Geophys. Res.: Atmospheres*, **117**, D22307,
458 <https://doi.org/10.1029/2012JD018261>, 2012.

459

460 Cooper, O. R., Schultz, M. G., Schröder, S., Chang, K.-L., Gaudel, A., Gerardo,
461 Benítez, C., Cuevas, E., Fröhlich, M., Galbally, I. E., Kubistin, D., Lu, X., Audra,
462 McClure-Begley, A., Molloy, S., Nédélec, P., O'Brien, J., Oltmans, S. J., Irina,
463 Petropavlovskikh, I., Ries, L., Senik, I., Sjöberg, K., Solberg, S., Spain, T. G.,
464 Spangl, W., Steinbacher, M., Tarasick, D., Thouret, V., and Xu, X.: Multi-decadal
465 surface ozone trends at globally distributed remote locations, *Elem Sci Anth*, **8**,
466 23, <https://doi.org/10.1525/elementa.420>, 2020.

467

468 Duncan, B. N., Lamsal, L. N., Thompson, A. M., Yoshida, Y., Lu, Z., Streets, D.
469 G., Hurwitz, M. M., and Pickering, K. E.: A space-based, high-resolution view of
470 notable changes in urban NO_x pollution around the world (2005–2014), *J.*
471 *Geophys. Res.*, **21**, 976-996, <https://doi.org/10.1002/2015JD024121>, 2016.

472

473 Emmons, L. K., Walters, S., Hess, P. G., Lamarque, J.-F., Pfister, G. G., Fillmore,



474 D., Granier, C., Guenther, A., Kinnison, D., Laepple, T., Orlando, J., Tie, X.,
475 Tyndall, G., Wiedinmyer, C., Baughcum, S. L., and Kloster, S.: Description and
476 evaluation of the Model for Ozone and Related chemical Tracers, version 4
477 (MOZART-4), *Geosci. Model Dev.*, 3, 43–67, [https://doi.org/10.5194/gmd-3-43-](https://doi.org/10.5194/gmd-3-43-2010)
478 2010, 2010.
479
480 Eyring, V.: Emissions from international shipping: 1. The last 50 years, *J.*
481 *Geophys. Res.*, 110, <https://doi.org/10.1029/2004JD005619>, 2005.
482
483 Fiore, A. M., West, J. J., Horowitz, L. W., Naik, V., and Schwarzkopf, M. D.:
484 Characterizing the tropospheric ozone response to methane emission controls
485 and the benefits to climate and air quality, *J. Geophys. Res.*, 113, D08307,
486 <https://doi.org/10.1029/2007JD009162>, 2008.
487
488 Fiore, A. M., Dentener, F. J., Wild, O., Cuvelier, C., Schultz, M. G., Hess, P.,
489 Textor, C., Schulz, M., Doherty, R. M., Horowitz, L. W., MacKenzie, I. A.,
490 Sanderson, M. G., Shindell, D. T., Stevenson, D. S., Szopa, S., van Dingenen,
491 R., Zeng, G., Atherton, C., Bergmann, D., Bey, I., Carmichael, G., Collins, W. J.,
492 Duncan, B. N., Faluvegi, G., Folberth, G., Gauss, M., Gong, S., Hauglustaine,
493 D., Holloway, T., Isaksen, I. S. A., Jacob, D. J., Jonson, J. E., Kaminski, J. W.,
494 Keating, T. J., Lupu, A., Marmer, E., Montanaro, V., Park, R. J., Pitari, G., Pringle,
495 K. J., Pyle, J. A., Schroeder, S., Vivanco, M. G., Wind, P., Wojcik, G., Wu, S.,
496 and Zuber, A.: Multimodel estimates of intercontinental source-receptor
497 relationships for ozone pollution, *J. Geophys. Res.*, 114, D04301 ,
498 <https://doi.org/10.1029/2008JD010816>, 2009.
499
500 Fleming, Z. L., Doherty, R. M., Schneidemesser, E. V ., Malley, C. S., Cooper,
501 O. R., Pinto, J. P ., Colette, A., Xu, X., Simpson, D., Schultz, M. G., Lefohn, A.
502 S., Hamad, S., Moolla, R., Solberg, S., and Feng, Z.: Tropospheric Ozone
503 Assessment Report: Present-day ozone distribution and trends relevant to
504 human health, *Elem. Sci. Anth.*, 6, p. 12, <https://doi.org/10.1525/elementa.273>,
505 2018.
506
507 Gao, J., Zhu, B., Xiao, H., Kang, H., Hou, X., and Shao, P.: A case study of
508 surface ozone source apportionment during a high concentration episode,
509 under frequent shifting wind conditions over the Yangtze River Delta, China, *Sci.*
510 *Total Environ.*, 544, 853-863, <https://doi.org/10.1016/j.scitotenv.2015.12.039>,
511 2016. Gao, Y., Fu, J. S., Drake, J. B., Lamarque, J. F., and Liu, Y.: The impact
512 of emission and climate change on ozone in the United States under
513 representative concentration pathways (RCPs), *Atmos. Chem. Phys.*, 13, 9607-
514 9621, <https://doi.org/10.5194/acp-13-9607-2013>, 2013.
515



- 516 Gaudel, A., Cooper, O. R. , Chang, K. L., Bourgeois, I., Ziemke, J. R., Strode,
517 S. A., Oman, L. D., Sellitto, P., Nédélec, P., Bolt, R., Thouret, V. and Granier, C.:
518 Aircraft observations since the 1990s reveal increases of tropospheric ozone at
519 multiple locations across the Northern Hemisphere, *Sci. Advance.*, 6,
520 <https://doi.org/10.1126/sciadv.aba8272>, 2020.
521
- 522 Gelaro, R., McCarty, W., Suárez, M. J., Todling, R., Molod, A., Takacs, L.,
523 Randles, C. A., Darmenov, A., Bosilovich, M. G., Reichle, R., Wargan, K., Coy,
524 L., Cullather, R., Draper, C., Akella, S., Buchard, V., Conaty, A., da Silva, A. M.,
525 Gu, W., Kim, G., Koster, R., Lucchesi, R., Merkova, D., Nielsen, J. E., Partyka,
526 G., Pawson, S., Putman, W., Rienecker, M., Schubert, S. D., Sienkiewicz, M.,
527 and Zhao, B.: The Modern-Era Retrospective Analysis for Research and
528 Applications, Version 2 (MERRA-2), *J. Climate*, 30, 5419–5454,
529 <https://doi.org/10.1175/JCLI-D-16-0758.1>, 2017.
530
- 531 Haagen-Smit, A. J.: Chemistry and Physiology of Los Angeles Smog, *Ind. Eng.*
532 *Chem.*, 44, 1342–1346, <https://doi.org/10.1021/ie50510a045>, 1952.
533
- 534 Hodnebrog, Ø., Berntsen, T. K., Dessens, O., Gauss, M., Grewe, V., Isaksen, I.
535 S. A., Koffi, B., Myhre, G., Olivie, D., Prather, M. J., Pyle, J. A., Stordal, F., Szopa,
536 S., Tang, Q., van Velthoven, P., Williams, J. E., and Ødemark, K.: Future impact
537 of non-land based traffic emissions on atmospheric ozone and OH – an
538 optimistic scenario and a possible mitigation strategy, *Atmos. Chem. Phys.*, 11,
539 11293–11317, <https://doi.org/10.5194/acp-11-11293-2011>, 2011.
540
- 541 Hoesly, R. M., Smith, S. J., Feng, L., Klimont, Z., Janssens-Maenhout, G.,
542 Pitkanen, T., Seibert, J. J., Vu, L., Andres, R. J., Bolt, R. M., Bond, T. C.,
543 Dawidowski, L., Kholod, N., Kurokawa, J.-I., Li, M., Liu, L., Lu, Z., Moura, M. C.
544 P., O'Rourke, P. R., and Zhang, Q.: Historical (1750–2014) anthropogenic
545 emissions of reactive gases and aerosols from the Community Emissions Data
546 System (CEDS), *Geosci. Model Dev.*, 11, 369–408,
547 <https://doi.org/10.5194/gmd-11-369-2018>, 2018.
548
- 549 Han, H., Liu, J., Yuan, H., Zhuang, B., Zhu, Y., Wu, Y., Yan, Y., and Ding, A.:
550 Characteristics of intercontinental transport of tropospheric ozone from Africa
551 to Asia, *Atmos. Chem. Phys.*, 18, 4251–4276, <https://doi.org/10.5194/acp-18-4251-2018>, 2018.
552
- 553
- 554 Hoor, P., Borken-Kleefeld, J., Caro, D., Dessens, O., Endresen, Ø., Gauss, M.,
555 Grewe, V., Hauglustaine, D. A., Isaksen, I. S. A., Jöckel, P., Lelieveld, J., Myhre,
556 G., Meijer, E. W., Olivie, D., Prather, M. J., Poberaj, C. S., Shine, K. P., Staehelin,
557 J., Tang, Q., Aardenne, J. v., Velthoven, P. F. J. v., and Sausen, R.: The impact



558 of traffic emissions on atmospheric ozone and OH: results from QUANTIFY,
559 Atmos. Chem. Phys., 9, 3113–3116, <https://doi.org/10.5194/acp-9-3113-2009>,
560 2009.
561
562 Jaffe, D. A., Cooper, O. R., Fiore, A. M., Henderson, B. H., Tonnesen, G. S.,
563 Russell, A. G., Henze, D. K., Langford, A. O., Lin, M., and Moore, T.: Scientific
564 assessment of background ozone over the U.S.: Implications for air quality
565 management, Elem. Sci. Anth, 6, 56, doi: <https://doi.org/10.1525/elementa.309>,
566 2018.
567
568 Johnson, C., Collins, W., Stevenson, D., and Derwent, R.: Relative roles of
569 climate and emissions changes on future tropospheric oxidant concentrations,
570 J. Geophys. Res.-Atmos., 104, 18631–18645,
571 <https://doi.org/10.1029/1999JD900204>, 1999.
572
573 Kasibhatla, P., Levy, H., Moxim, W. J., Pandis, S. N., Corbett, J. J., Peterson,
574 M. C., Honrath, R. E., Frost, G. J., Knapp, K., Parrish, D. D., and Ryerson, T.
575 B.: Do emissions from ships have a significant impact on concentrations of
576 nitrogen oxides in the marine boundary layer?, Geophys. Res. Lett., 27, 2229–
577 2232, <https://doi.org/10.1029/2000gl011387>, 2000.
578
579 Koffi, B., Szopa, S., Cozic, A., Hauglustaine, D., and van Velthoven, P.: Present
580 and future impact of aircraft, road traffic and shipping emissions on global
581 tropospheric ozone, Atmos. Chem. Phys., 10, 11681–11705,
582 <https://doi.org/10.5194/acp-10-11681-2010>, 2010.
583
584 Koo, B., Wilson, G. M., Morris, R., Dunker, A. M., and Yarwood, G.: Comparison
585 of Source Apportionment and Sensitivity Analysis in a Particulate Matter Air
586 Quality Model, Environ. Sci. Technol., 43, 6669–6675,
587 <https://doi.org/10.1021/es9008129>, 2009.
588
589 Lamarque, J.-F., Emmons, L. K., Hess, P. G., Kinnison, D. E., Tilmes, S., Vitt,
590 F., Heald, C. L., Holland, E. A., Lauritzen, P. H., Neu, J., Orlando, J. J., Rasch,
591 P. J., and Tyndall, G. K.: CAM-chem: description and evaluation of interactive
592 atmospheric chemistry in the Community Earth System Model, Geosci. Model
593 Dev., 5, 369–411, <https://doi.org/10.5194/gmd-5-369-2012>, 2012.
594
595 Lin, M., Horowitz, L. W., Payton, R., Fiore, A. M., and Tonnesen, G. S.: US
596 surface ozone trends and extremes from 1980 to 2014: quantifying the roles of
597 rising Asian emissions, domestic controls, wildfires, and climate, Atmospheric
598 Chemistry and Physics, 17, 2943–2970, [https://doi.org/10.5194/acp-17-2943-](https://doi.org/10.5194/acp-17-2943-2017)
599 2017, 2017.



- 600
601 Lupaşcu, A. and Butler, T.: Source attribution of European surface O₃ using a
602 tagged O₃ mechanism, *Atmos. Chem. Phys.*, 19, 14535–14558,
603 <https://doi.org/10.5194/acp-19-14535-2019>, 2019.
- 604
605 Müller-Casseres, E., Edelenbosch, O. Y., Szklo, A., Schaeffer, R., and van
606 Vuuren, D. P.: Global futures of trade impacting the challenge to decarbonize
607 the international shipping sector, *Energy*, 237, 121547,
608 <https://doi.org/10.1016/j.energy.2021.121547>, 2021
- 609
610 Myhre, G., D. Shindell, F.-M. Bréon, W. Collins, J. Fuglestedt, J. Huang, D.
611 Koch, J.-F. Lamarque, D. Lee, B. Mendoza, T. Nakajima, A. Robock, G.
612 Stephens, T. Takemura and H. Zhang, 2013: Anthropogenic and Natural
613 Radiative Forcing. In: *Climate Change 2013: The Physical Science Basis.*
614 Contribution of Working Group I to the Fifth Assessment Report of the
615 Intergovernmental Panel on Climate Change [Stocker, T.F., D. Qin, G.-K.
616 Plattner, M. Tignor, S.K. Allen, J. Boschung, A. Nauels, Y. Xia, V. Bex and P.M.
617 Midgley (eds.)]. Cambridge University Press, Cambridge, United Kingdom and
618 New York, NY, USA, 2013.
- 619
620 O'Neill, B. C., Tebaldi, C., van Vuuren, D. P., Eyring, V., Friedlingstein, P., Hurtt,
621 G., Knutti, R., Kriegler, E., Lamarque, J.-F., Lowe, J., Meehl, G. A., Moss, R.,
622 Riahi, K., and Sanderson, B. M.: The Scenario Model Intercomparison Project
623 (ScenarioMIP) for CMIP6, *Geosci. Model Dev.*, 9, 3461–3482,
624 <https://doi.org/10.5194/gmd-9-3461-2016>, 2016.
- 625
626 Price, C., Penner, J., and Prather, M.: NO_x from lightning 1, Global distribution
627 based on lightning physics, *J. Geophys. Res.*, 102, 5929–5941,
628 <https://doi.org/10.1029/96JD03504>, 1997.
- 629
630 Seinfeld, J. H. and Pandis, S. N.: *Atmospheric Chemistry and Physics: From*
631 *Air Pollution to Climate Change*, J. Wiley, Hoboken, N.J., 2006.
- 632
633 Simon, H., Reff, A., Wells, B., Xing, J., and Frank, N.: Ozone trends across the
634 United States over a period of decreasing NO_x and VOC emissions, *Environ.*
635 *Sci. Technol.*, 49, 186–195, <https://doi.org/10.1021/es504514z>, 2015.
- 636
637 Shen, L. and Mickley, L. J.: Effects of El Niño on summertime ozone air quality
638 in the eastern United States *Geophys. Res. Lett.* 44, 12543–50,
639 <https://doi.org/10.1002/2017GL076150>, 2017.
- 640
641 Stevenson, D. S., Dentener, F. J., Schultz, M. G., Ellingsen, K., van Noije, T. P.



642 C., Wild, O., Zeng, G., Amann, M., Atherton, C. S., Bell, N., Bergmann, D. J.,
643 Bey, I., Butler, T., Cofala, J., Collins, W. J., Derwent, R. G., Doherty, R. M.,
644 Drevet, J., Eskes, H. J., Fiore, A. M., Gauss, M., Hauglustaine, D. A., Horowitz,
645 L. W., Isaksen, I. S. A., Krol, M. C., Lamarque, J.-F., Lawrence, M. G.,
646 Montanaro, V., Müller, J.-F., Pitari, G., Prather, M. J., Pyle, J. A., Rast, S.,
647 Rodriguez, J. M., Sanderson, M. G., Savage, N. H., Shindell, D. T., Strahan, S.
648 E., Sudo, K., and Szopa, S.: Multimodel ensemble simulations of present-day
649 and near-future tropospheric ozone. *J. Geophys. Res.*, 111, D08301.
650 <https://doi.org/10.1029/2005JD006338>, 2006.

651

652 Sudo, K., and Akimoto, H.: Global source attribution of tropospheric ozone:
653 Long-range transport from various source regions, *J. Geophys. Res.*, 112,
654 D12302, <https://doi.org/10.1029/2006JD007992>, 2007.

655

656 Szopa, S., V. Naik, B. Adhikary, P. Artaxo, T. Berntsen, W.D. Collins, S. Fuzzi,
657 L. Gallardo, A. Kiendler-Scharr, Z. Klimont, H. Liao, N. Unger, and P. Zanis:
658 Short-Lived Climate Forcers. In *Climate Change 2021: The Physical Science
659 Basis. Contribution of Working Group I to the Sixth Assessment Report of the
660 Intergovernmental Panel on Climate Change* [Masson-Delmotte, V., P. Zhai,
661 A. Pirani, S.L. Connors, C. Péan, S. Berger, N. Caud, Y. Chen, L. Goldfarb,
662 M.I. Gomis, M. Huang, K. Leitzell, E. Lonnoy, J.B.R. Matthews, T.K.
663 Maycock, T. Waterfield, O. Yelekçi, R. Yu, and B. Zhou (eds.)]. Cambridge
664 University Press, Cambridge, United Kingdom and New York, NY, USA, pp.
665 817–922, <https://doi.org/10.1017/9781009157896.008>, 2021.

666

667 Tilmes, S., Lamarque, J. F., Emmons, L. K., Kinnison, D. E., Marsh, D., Garcia,
668 R. R., Smith, A. K., Neely, R. R., Conley, A., Vitt, F., Val Martin, M., Tanimoto,
669 H., Simpson, I., Blake, D. R., and Blake, N.: Representation of the Community
670 Earth System Model (CESM1) CAM4-chem within the Chemistry-Climate
671 Model Initiative (CCMI), *Geosci. Model Dev.*, 9, 1853–1890,
672 <https://doi.org/10.5194/gmd-9-1853-2016>, 2016.

673

674 Tilmes, S., Lamarque, J. F., Emmons, L. K., Kinnison, D. E., Ma, P. L., Liu, X.,
675 Ghan, S., Bardeen, C., Arnold, S., Deeter, M., Vitt, F., Ryerson, T., Elkins, J. W.,
676 Moore, F., Spackman, J. R., and Val Martin, M.: Description and evaluation of
677 tropospheric chemistry and aerosols in the Community Earth System Model
678 (CESM1.2), *Geosci. Model Dev.*, 8, 1395–1426, [https://doi.org/10.5194/gmd-8-
679 1395-2015](https://doi.org/10.5194/gmd-8-1395-2015), 2015.

680

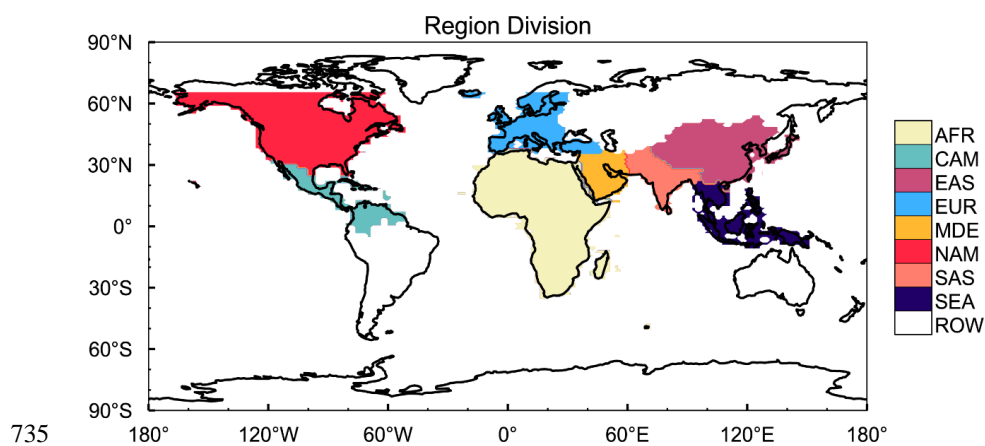
681 van Marle, M. J. E., Kloster, S., Magi, B. I., Marlon, J. R., Daniau, A.-L., Field,
682 R. D., Arneth, A., Forrest, M., Hantson, S., Kehrwald, N. M., Knorr, W., Lasslop,
683 G., Li, F., Mangeon, S., Yue, C., Kaiser, J. W., and van der Werf, G. R.: Historic



- 684 global biomass burning emissions for CMIP6 (BB4CMIP) based on merging
685 satellite observations with proxies and fire models (1750–2015), *Geosci. Model*
686 *Dev.*, 10, 3329–3357, <https://doi.org/10.5194/gmd-10-3329-2017>, 2017.
687
- 688 von Glasow, R., Lawrence, M. G., Sander, R., and Crutzen, P. J.: Modeling the
689 chemical effects of ship exhaust in the cloudfree marine boundary layer, *Atmos.*
690 *Chem. Phys.*, 3, 233–250, <https://doi.org/10.5194/acp-3-233-2003>, 2003.
691
- 692 Wang, H., Rasch, P. J., Easter, R. C., Singh, B., Zhang, R., Ma, P.-L., Qian, Y.,
693 Ghan, S. J., and Beagley, N.: Using an explicit emission tagging method in
694 global modeling of source-receptor relationships for black carbon in the Arctic:
695 Variations, sources, and transport pathways, *J. Geophys. Res.*, 119, 12888–
696 12909, <https://doi.org/10.1002/2014JD022297>, 2014.
697
- 698 Xing, J., Pleim, J. E., Mathur, R., Pouliot, G., Hogrefe, C., Gan, C.-M., and Wei,
699 C.: Historical gaseous and primary aerosol emissions in the United States from
700 1990 to 2010, *Atmos. Chem. Phys.*, 13, 7531–7549,
701 <https://doi.org/10.5194/acp-13-7531-2013>, 2013.
702
- 703 Yang, Y., Li, M., Wang, H., Li, H., Wang, P., Li, K., Gao, M., and Liao, H.: ENSO
704 modulation of summertime tropospheric ozone over China, *Environ. Res. Lett.*,
705 17, 034020, <https://doi.org/10.1088/1748-9326/ac54cd>, 2022.
706
- 707 Yang, Y., Liao, H., and Li, J.: Impacts of the East Asian summer monsoon on
708 interannual variations of summertime surface-layer ozone concentrations over
709 China, *Atmos. Chem. Phys.*, 14, 6867–6879, <https://doi.org/10.5194/acp-14-6867-2014>, 2014.
710
- 711
- 712 Yang, Y., Wang, H., Smith, S. J., Zhang, R., Lou, S., Yu, H., Li, C., and Rasch,
713 P. J.: Source apportionments of aerosols and their direct radiative forcing and
714 long-term trends over continental United States, *Earth's Future*, 6, 793–808,
715 <https://doi.org/10.1029/2018EF000859>, 2018.
716
- 717 Zhang, L., Jacob, D. J., Boersma, K. F., Jaffe, D. A., Olson, J. R., Bowman, K.
718 W., Worden, J. R., Thompson, A. M., Avery, M. A., Cohen, R. C., Dibb, J. E.,
719 Flock, F. M., Fuelberg, H. E., Huey, L. G., McMillan, W. W., Singh, H. B., and
720 Weinheimer, A. J.: Transpacific transport of ozone pollution and the effect of
721 recent Asian emission increases on air quality in North America: an integrated
722 analysis using satellite, aircraft, ozonesonde, and surface observations, *Atmos.*
723 *Chem. Phys.*, 8, 6117–6136, <https://doi.org/10.5194/acp-8-6117-2008>, 2008.
724
- 725 Zhang, Y., Cooper, O. R., Gaudel, A., Nedelec, P., Ogino, S. Y., Thompson, A.



726 M., and West, J. J.: Tropospheric ozone change from 1980 to 2010 dominated
727 by equatorward redistribution of emissions, *Nat. Geosci.*, 9, 875-879,
728 <https://doi.org/10.1038/ngeo2827>, 2016.
729
730 Zhang, Y., West, J. J., Emmons, L. K., Flemming, J., Jonson, J. E., Lund, M. T.,
731 Sekiya, T., Sudo, K., Gaudel, A., Chang, K. L., Nédélec, P., and Thouret, V.:
732 Contributions of World Regions to the Global Tropospheric Ozone Burden
733 Change From 1980 to 2010, *Geophys. Res. Lett.*, 48,
734 <https://doi.org/10.1029/2020GL089184>, 2021.

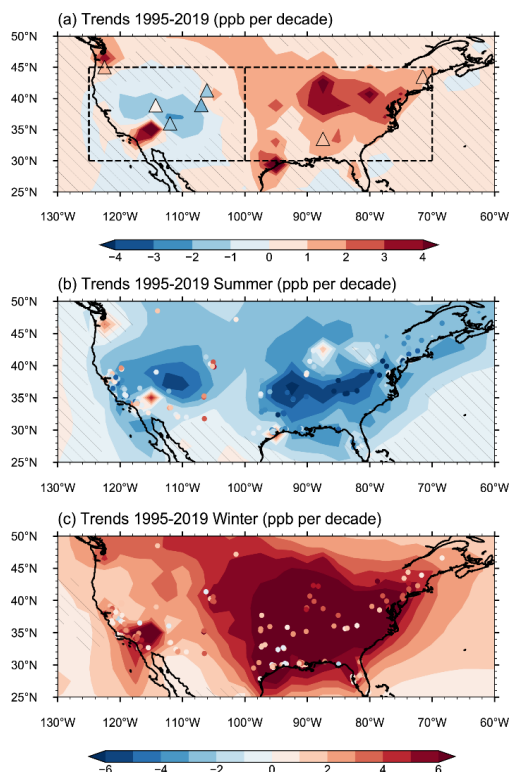


735

736

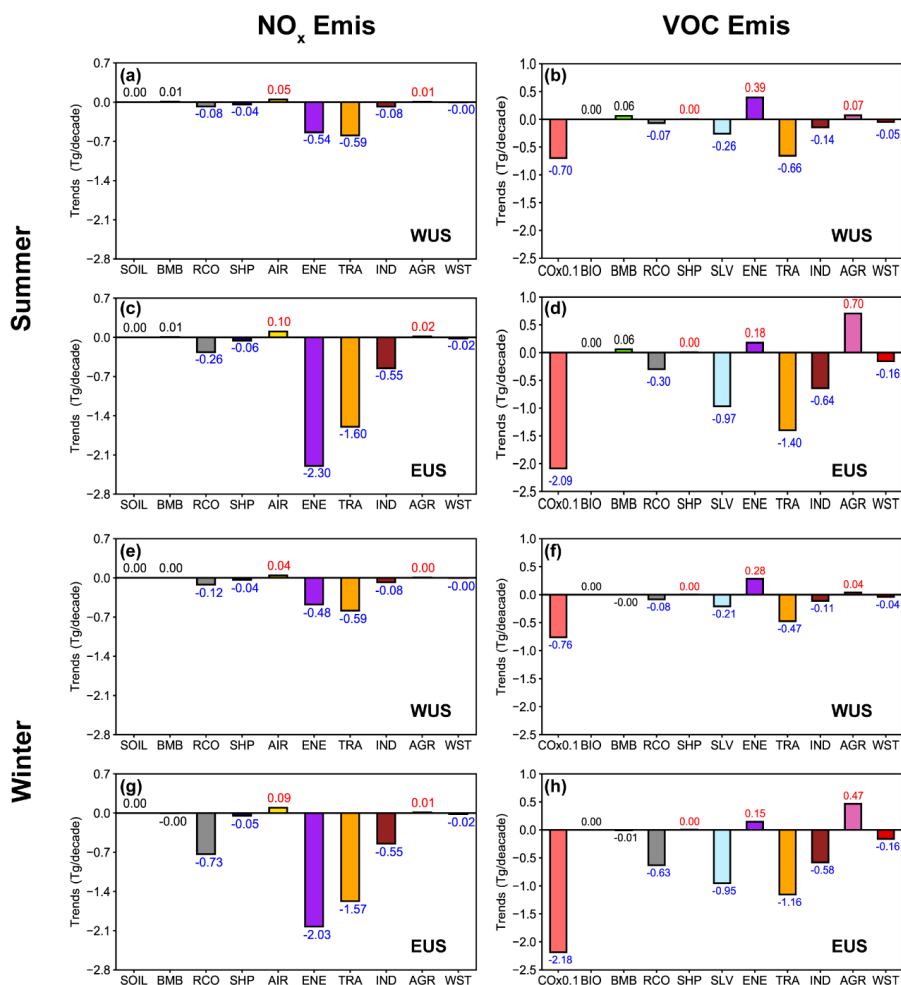
737 **Figure 1.** Source regions that are selected for O₃ source tagging in this study,
738 include Africa (AFR), Central America (CAM), East Asia (EAS), Europe (EUR),
739 Middle East (MDE), North America (NAM), South Asia (SAS), Southeast Asia
740 (SEA) and rest of the world (ROW).

741



742
743
744
745
746
747
748
749
750
751
752
753

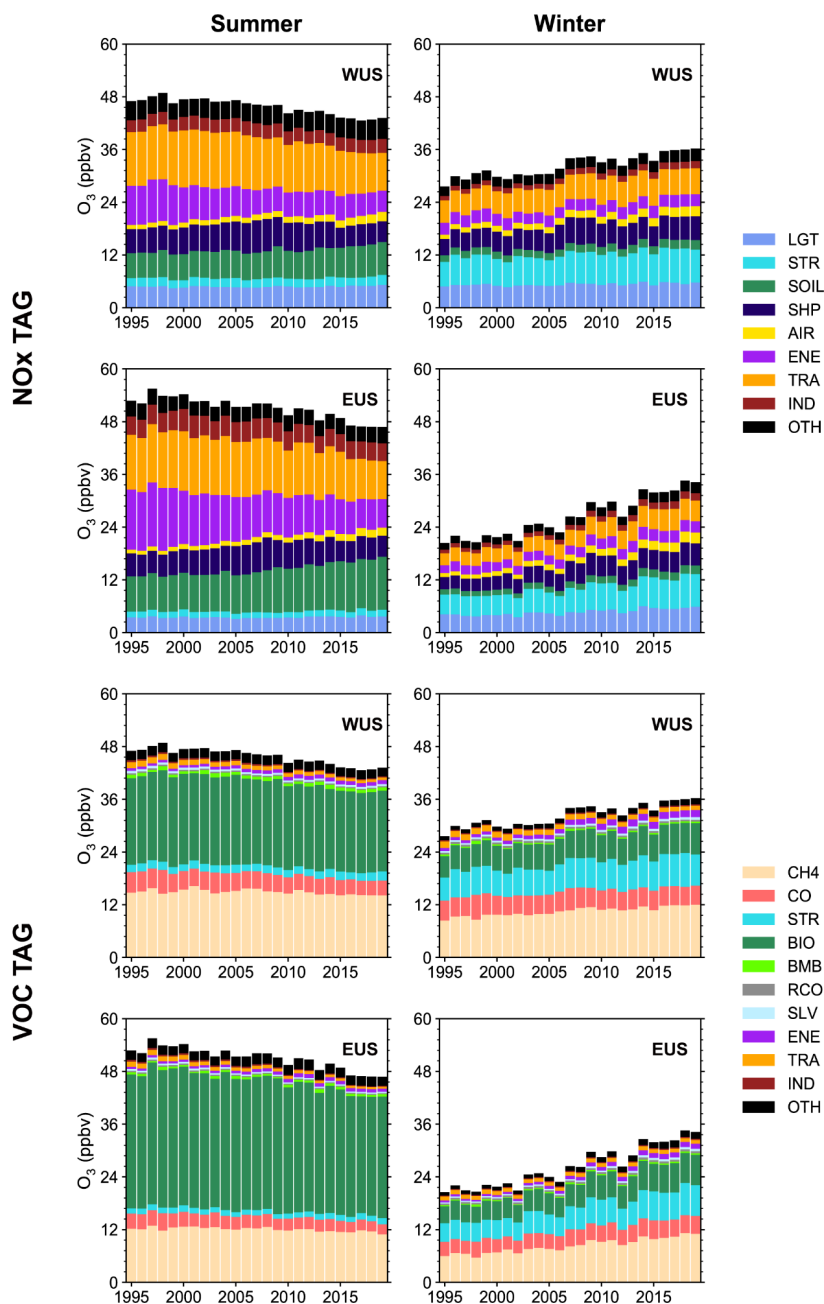
Figure 2. Linear trends (ppb/decade) of simulated (contours) and observed (color-filled markers) (a) annual, (b) JJA and (c) DJF mean near-surface O₃ concentrations during 1995–2019. Areas without hatches indicate statistical significance with 95% confidence. The boxes in (a) mark the western U.S. (WUS, 100–125°W, 30–45°N) and eastern U.S. (EUS, 70–100°W, 30–45°N), respectively. The observed annual O₃ concentration trends in (a) are derived from IPCC AR6, based on Cooper et al. (2020) and Gaudel et al. (2020) over 1995–2017. The observed seasonal O₃ concentration trends in (b) and (c) are calculated based on the U.S. EPA O₃ measurements over 1995–2019.



754

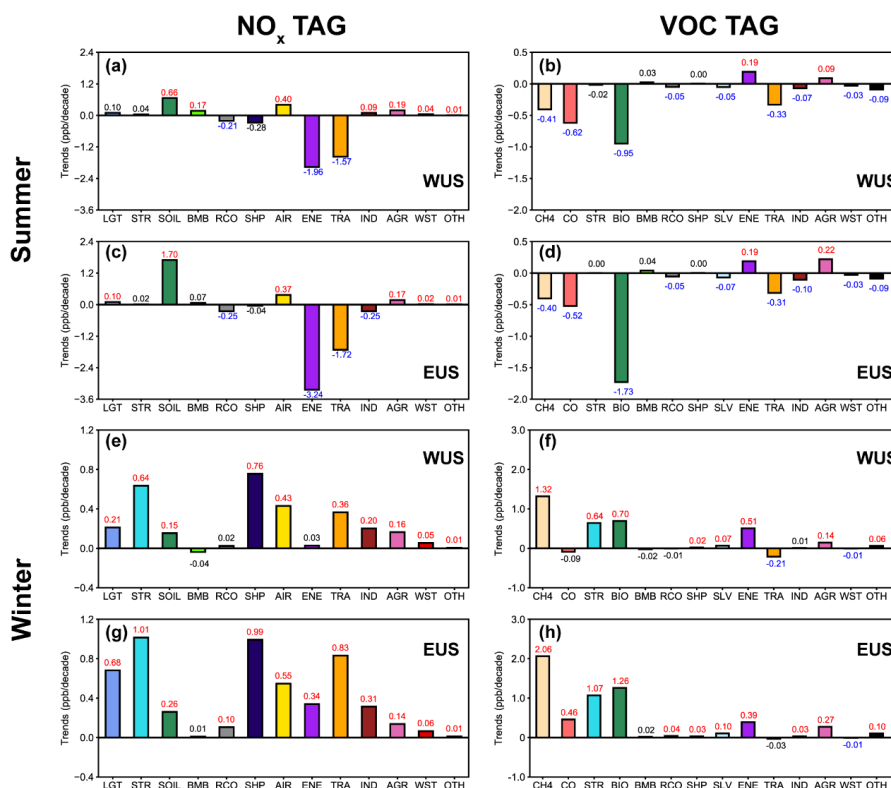
755

756 **Figure 3.** Linear trends of NO_x and reactive carbon emissions from various
 757 sectors in summer and winter over WUS and EUS. The increasing and
 758 decreasing trends marked with red and blue values, respectively, indicate
 759 statistical significance with 95% confidence.



760
761

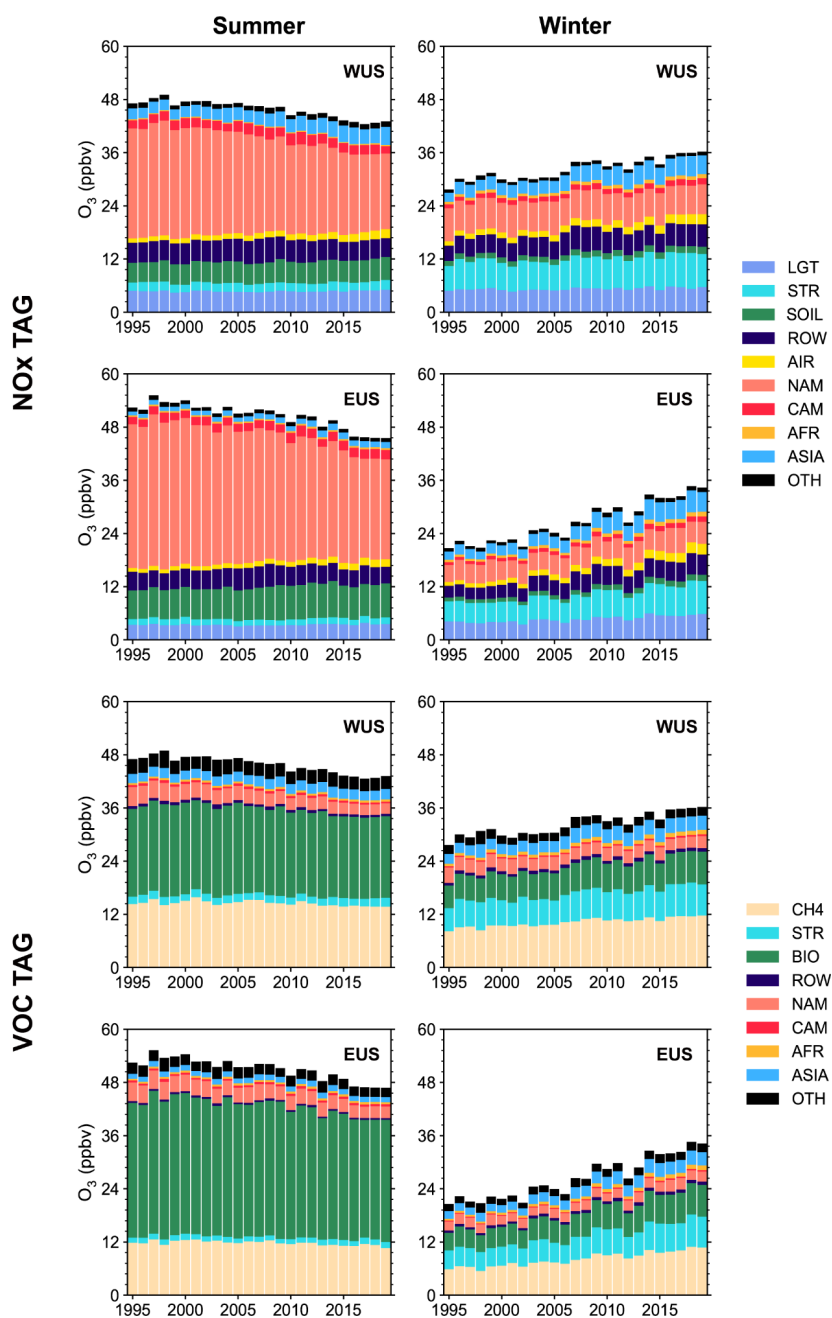
762 **Figure 4.** Time series of near-surface O₃ concentrations (ppb) averaged over
763 WUS and EUS contributed by NO_x and reactive carbon emissions from
764 different sectors in summer and winter during 1995–2019. Sources with small
765 contributions are combined and shown as OTH.



766

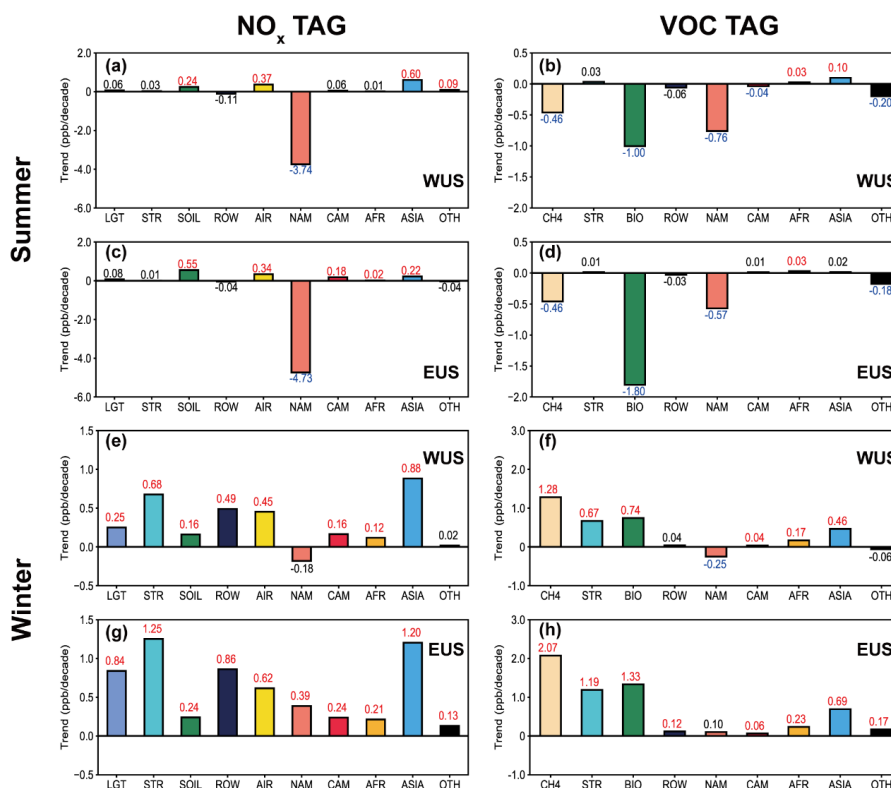
767

768 **Figure 5.** Linear trends (ppb/decade) of near-surface O₃ concentrations in
 769 summer and winter over WUS and EUS contributed by the NO_x (left) and
 770 reactive carbon (right) emissions from various sectors (color bars). The
 771 increasing and decreasing trends marked with red and blue color numbers,
 772 respectively, indicate statistical significance with 95% confidence. Other
 773 sources having small contributions are combined and shown as OTH.



774
775

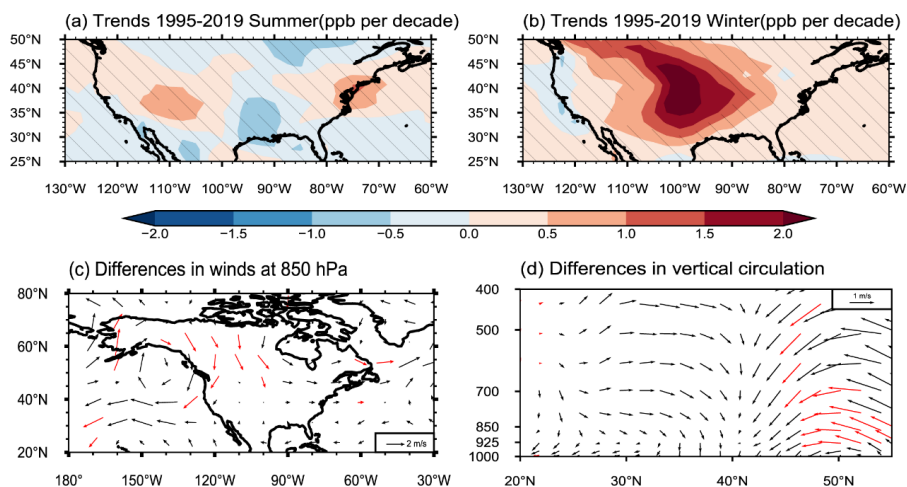
776 **Figure 6.** Time series of near-surface O_3 concentrations (ppb) averaged over
777 WUS and EUS contributed by NO_x and reactive carbon emissions from different
778 source regions in summer and winter during 1995–2019. Sources with small
779 contributions are combined and shown as OTH.



780

781

782 **Figure 7.** Linear trends (ppb/decade) of near-surface O₃ concentrations in
 783 summer and winter over WUS and EUS contributed by the NO_x (left) and
 784 reactive carbon (right) emissions from various source regions (color bars). The
 785 increasing and decreasing trends marked with red and blue color numbers,
 786 respectively, indicate statistical significance with 95% confidence. Contributions
 787 from source regions EAS, SAS and SEA are combined to ASIA. Other sources
 788 having small contributions are combined and shown as OTH.



789

790

791 **Figure 8.** Linear trends (ppb/decade) of simulated (a) JJA and (b) DJF mean
792 near-surface O₃ concentrations during 1995–2019. Differences between the
793 first (1995–1999) and last (2015–2019) five years during 1995–2019 (last–
794 first) in DJF mean (c) 850 hPa horizontal winds and (d) meridional winds and
795 vertical velocity averaged over 90–105°W. Areas without hatches in (a) and
796 (b) and red arrows in (c) and (d) indicate statistical significance with 95%
797 confidence. All results are from the MET experiments.